Finite element modeling of the rolling behavior of a polyurethane sphere for low-cost seismic isolation application

Author(s):
Reyes, Sergio; Vassiliou, Michalis F.; Agathos, Konstantinos; Konstantinidis, Dimitrios

Publication date:
2023-10

Permanent link:
https://doi.org/10.3929/ethz-b-000615832

Originally published in:
COMPDYN Proceedings, https://doi.org/10.7712/120123.10383.20677

COMPDYN 2023
9th ECCOMAS Thematic Conference on
Computational Methods in Structural Dynamics and Earthquake Engineering
M. Papadrakakis, M. Fragiadakis (eds.)
Athens, Greece, 12-14 June 2023

FINITE ELEMENT MODELING OF THE ROLLING BEHAVIOR OF A POLYURETHANE SPHERE FOR LOW-COST SEISMIC ISOLATION APPLICATIONS

Sergio I. Reyes[1], Michalis F. Vassiliou[2], Konstantinos Agathos[3], Dimitrios Konstantinidis[4]

[1] Institute of Structural Engineering, Swiss Federal Institute of Technology (ETH) Zurich, CH.
e-mail: sergio.reyes@ibk.baug.ethz.ch

[2] Institute of Structural Engineering, Swiss Federal Institute of Technology (ETH) Zurich, CH.
e-mail: vassiliou@ibk.baug.ethz.ch

[3] College of Engineering, Mathematics, and Physical Sciences, University of Exeter, UK.
e-mail: k.agathos@exeter.ac.uk

[4] Department of Civil and Environmental Engineering, University of California, Berkeley, US.
e-mail: konstantinidis@berkeley.edu

Abstract

This paper presents the experimental test and finite element modeling of the rolling behavior of a very hard (95 Shore A) polyurethane elastomeric sphere that can be used to construct low-cost seismic isolation systems. A small-amplitude rolling test was performed at the component level on a polyurethane sphere to validate the finite element simulations. The considered material model parameters were based on those presented by the authors in a previous study. The constitutive model was based on the parallel rheological framework considering three mechanisms: one mechanism representing the equilibrium behavior of the material (modeled with a hyperelastic constitutive law), and two mechanisms representing the rate-dependence at two different time scales (modeled as a hyperelastic spring in series with a nonlinear viscoplastic dashpot element). The results showed a good overall agreement between the rolling test and the numerical simulation; however, better material characterization is required to improve the results in terms of the energy dissipated and the shape of the hysteretic loops. Moreover, additional numerical simulations need to be conducted to understand the deformation mechanism within the ball, and thus select appropriate testing protocols for calibrating new material parameters.

Keywords: low-cost seismic isolation, finite element, Bergstrom Boyce, hyperelastic material, hyperelasticity, rubber modeling, parallel rheological framework, testing protocol.

1 INTRODUCTION

Seismic isolation is a mature earthquake protection method widely used in earthquake-prone countries. However, its application in the developing world is still limited mainly due to the high cost of isolation devices (e.g., rubber bearings or friction pendulum sliders). Several studies have focused on ways of making this technology more affordable by proposing Fiber Reinforced Elastomeric Isolators (FREIs) [1–5]. These isolators replace the steel shims in traditional rubber bearings with fiber sheets, reducing their weight and total installation costs.

More recently, rolling-type isolation systems [5] have also been explored as effective low-cost solutions. Tsai et al. [6,7] experimentally studied the concept of an Elastomeric-Ball Pendulum System (EBPS) to protect sensitive equipment using balls covered by a damping material (e.g., rubber). The results showed that covering the steel ball with a flexible and dissipative material has mainly two beneficial effects: i) provides energy dissipation to the system, thus reducing the displacements and the required size of the isolation device, and ii) eliminates the abrasion produced on the surfaces when rolling a pure steel ball. This latter benefit may be particularly relevant when the rolling surface is not steel, e.g., concrete, since the high-stress concentration would cause the indentation of the steel ball and damage the rolling surface.

Cilsalar and Constantinou [8,9] further studied the EBPS with larger spheres and loads, aiming to explore its application for larger and heavier structures. Later, Katsamakas and Vassiliou [10,11] performed additional tests on 100 mm Thermoplastic Polyurethane (TPU) balls with and without a steel core, reaching larger rolling displacements. The latter tests highlighted the relevance of creep on the force-deformation relationship of the system, showing that the system behavior is more complicated than that of a rigid sphere rolling on a spherical surface. The elastomeric material creeps under vertical loads, develops flat spots against the top and bottom support surfaces, and becomes egg-shaped. When it rolls, its oblong shape results in non-smooth rolling motion causing a vertical oscillation that affects the global force-deformation relationship of the system. Early research on this subject addressed this issue by using an auxiliary system to support the vertical loads before the earthquake strikes [6], but its effectiveness for higher loads and concrete rolling surfaces has not been validated and may increase the cost of the system.

Despite all these studies, no accurate numerical simulations (e.g., finite element simulation) have yet been performed to understand and quantify the behavior of a rolling elastomeric ball for seismic applications. The complexity of such simulations lies in the complex mechanical behavior of elastomers. Depending on the exact material composition, it may exhibit a strongly nonlinear elastic and rate-dependent dissipative nature that will govern the system rolling behavior. Therefore, modeling such behavior requires a material constitutive law that considers all the elastomeric material nonlinear phenomena.

This paper presents the finite element simulation of an EBPS considering a TPU ball rolling on flat surfaces and its comparison with an experimental test. The TPU material was modeled using a parallel rheological framework with material parameters based on a previous study [12]. First, the constitutive equations of the model with the respective chosen parameters are presented. Then, the finite element model is described with all the relevant aspects for the simulation. Finally, the model is validated against experimental results.

2 CONSTITUTIVE MODEL AND PARAMETER CALIBRATION

2.1 Description of the constitutive model

The constitutive model and parameters considered herein are based on the study presented by Reyes et al. [12]. Figure 1 presents the one-dimensional rheological representation of the model. It consists of a three-mechanism model: one hyperelastic mechanism (H) representing the nonlinear elastic equilibrium path of the material, and two hyperelastic-viscoplastic mechanisms (P_1 and P_2) to represent the rate dependence of the material at two different timescales (i.e., represent the cyclic energy dissipation and the microstructural relaxation, respectively). The mechanism H is modeled through a nonlinear spring with a hyperelastic constitutive law. The mechanisms P_1 and P_2 are modeled as a hyperelastic spring in series with a nonlinear viscoplastic dashpot element. No temperature dependence is considered in the model.

Assuming an incompressible material, the Cauchy stress on any of the mechanisms can be computed directly as [13]:

$$\boldsymbol{\sigma} = 2\left(\frac{\partial W}{\partial I_1} + \frac{\partial W}{\partial I_2} I_1\right)\boldsymbol{B} - 2\frac{\partial W}{\partial I_2}\boldsymbol{B}^2 - p\boldsymbol{I} \tag{1}$$

where W is the strain-energy density function of the hyperelastic model considered in the spring of the mechanism, I_i is the i^{th} invariant of the left Cauchy-Green tensor $\mathbf{B}=\mathbf{F}\mathbf{F}^{\mathrm{T}}$, p is the hydrostatic pressure determined from the boundary conditions, and $\mathbf{I}$ is the identity matrix. Notice that $W=W_{dev}$ for practical purposes because of the incompressibility assumption and the independence of the volumetric part with respect to I_1 and I_2.

The hyperelastic spring of mechanism H (i.e., equilibrium path) is modeled with the incompressible Yeoh hyperelastic model [14]. This model corresponds to a phenomenological third-order polynomial that depends only on the first invariant I_1 of the left Cauchy-Green deformation tensor. The strain-energy density function of this model is:

$$W = C_{10}\left(I_1 - 3\right) + C_{20}\left(I_1 - 3\right)^2 + C_{30}\left(I_1 - 3\right)^3 \tag{2}$$

where C_{10}, C_{20}, and C_{30} are the parameters of the model.

The hyperelastic spring in the hyperelastic-viscoplastic mechanisms is modeled with the Arruda-Boyce (AB) hyperelastic model [15], also known as the Eight-Chain model. The strain energy density function of the AB model can be expressed as a series expansion, yielding the following expression [16]:

$$W = nkT_i\left[\frac{1}{2}\left(I_1 - 3\right) + \frac{1}{20N_i}\left(I_1^{\,2} - 9\right) + \frac{12}{1050N_i^{\,2}}\left(I_1^{\,3} - 27\right) + \frac{19}{7000N_i^{\,3}}\left(I_1^{\,4} - 81\right) + \frac{519}{673750N_i^{\,4}}\left(I_1^{\,5} - 243\right)\right] \tag{3}$$

where nkT_i and N_i are the model parameters, representing the initial modulus and limiting chain extensibility, respectively. Here, I_1 also corresponds to the first invariant of the left Cauchy-Green deformation tensor.

The nonlinear viscoplastic dashpot element is considered with the viscous flow rule used in the MSC MARC software [16]:

$$\dot{\gamma}_i = A_i\left[\lambda_{chain} - 1 + \xi\right]^{C_i}\left(\tau\right)^{m_i} \tag{4}$$

where A_i, C_i, and m_i are the model parameters, $\lambda_{chain} = \sqrt{tr\,\mathbf{B}_p/3}$ is the effective distortional chain stretch, ξ is a small positive constant (e.g., 5e-3) for stability in undeformed configurations (i.e., $\lambda_{chain} \approx 1$), and τ is the effective stress driving the viscous flow. This flow rule has

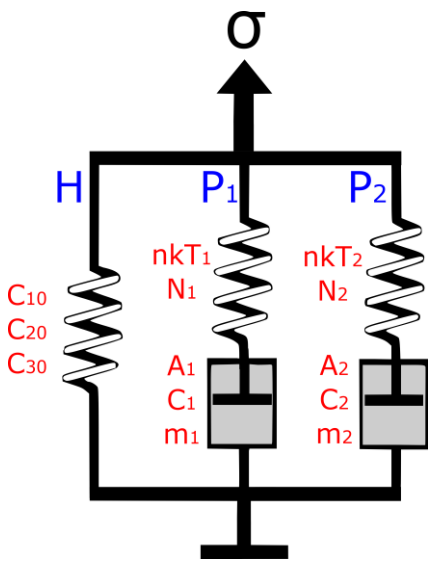

Figure 1: One-dimensional rheological representation of the three-mechanism model considered to represent the TPU material.

Mechanism	Parameter [units]	Value
Equilibrium path (Mechanism H)	C_{10} [MPa]	18.81
	C_{20} [MPa]	-0.46
	C_{30} [MPa]	0.16
Mechanism P_1	nkT_1 [MPa]	2.15
	N_1 [-]	2.10
	A_1 [MPa^{-1} s^{-1}]	0.2015
	C_1 [-]	-1.0
	m_1 [-]	3.60
Mechanism P_2	nkT_2 [MPa]	10.30
	N_2 [-]	3.80
	A_2 [MPa^{-1} s^{-1}]	1.30
	C_2 [-]	-1.00
	m_2 [-]	2.50

Table 1: Example of the construction of one table.

been widely used for representing the nonlinear time-dependent large-strain behavior of elastomeric materials [13,17–21].

The model considers the multiplicative decomposition of the deformation gradient acting on each hyperelastic-viscoplastic mechanism P_1 and P_2 (i.e., $\lambda_i=\lambda_i^e\lambda_i^p$), where the elastic stretch λ_i^e is associated with the hyperelastic spring (i.e., the AB model) and the plastic stretch λ_i^p with the nonlinear viscoplastic dashpot element. The algorithmic treatment for the time-step integration can be found elsewhere [13]. Table 1 presents the values considered for all the model parameters based on a previous study [12]; only the values of the parameters A_i were modified to have a better agreement with the tests in terms of energy dissipation.

3 EXPERIMENTAL TESTS AND NUMERICAL SIMULATION

3.1 Description of the experimental test

Figure 2 shows an overview of the experimental setup used for the test. It comprises a closed frame with one horizontal and two vertical actuators connected to a rigid steel beam. A concrete plate was attached below the steel beam (i.e., the top plate in Figure 2), corresponding to one of the surfaces where the ball was rolled. Another concrete plate was attached to the frame (i.e., the bottom plate in Figure 2), and a five-DOF loadcell was mounted below to measure the reaction forces. The displacement of the top plate was measured with an optical measurement system using sensors attached to it.

The performed test involved placing the TPU ball between the concrete plates, applying a vertical force of 12.5 kN, and applying to the top plate the lateral displacement protocol shown in Figure 3 (i.e., the motion of the horizontal actuator was displacement controlled). The motion of vertical actuators was force controlled to keep the vertical load constant while avoiding the rotation of the top plate. Restrainers prevented the out-of-plane motion of the top plate.

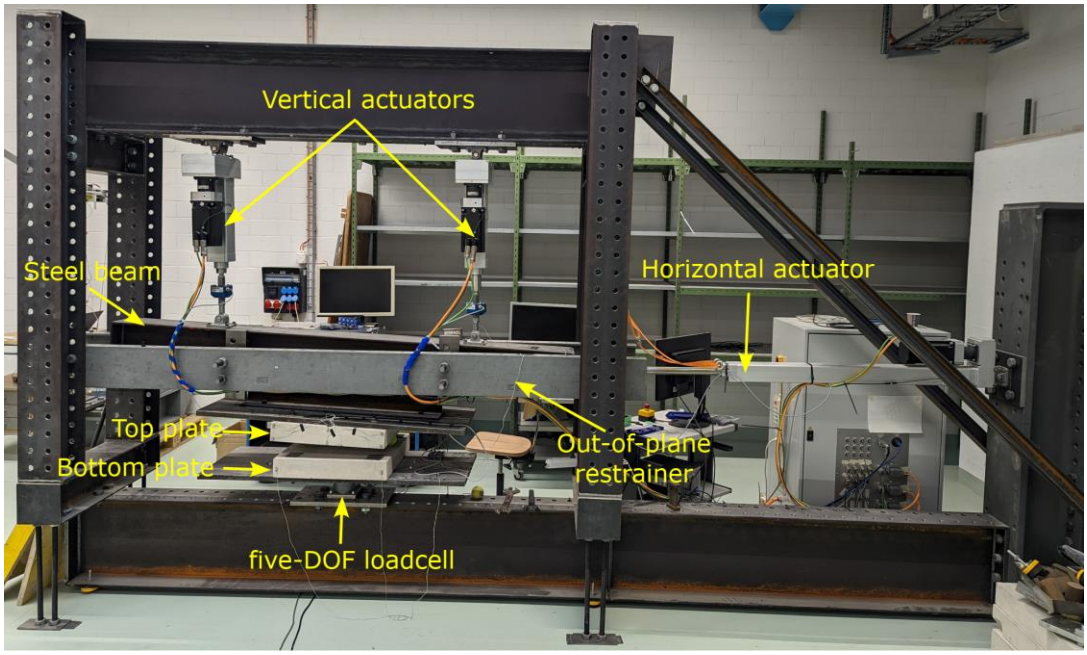

Figure 2: Experimental setup. (Top plate is rotated because the setup is turned off)

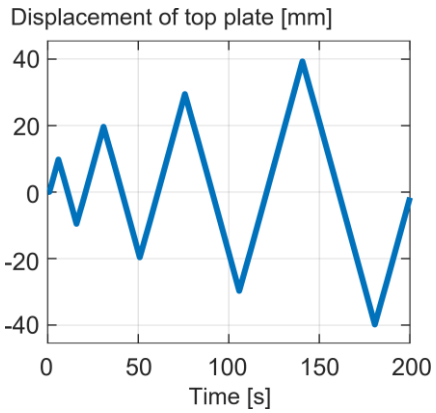

Figure 3: Applied lateral displacement on the top concrete plate.

3.2 Description of the finite element model

Figure 4 shows the finite element model constructed in MSC Marc software [22]. The model consists of the 100 mm diameter ball rolling between two rigid-like plates (representing the top and bottom concrete plates). Half of the model was considered for computational efficiency (i.e., taking advantage of the model symmetry). The final mesh size was chosen through convergence sensitivity (i.e., start with a coarse mesh and refine it until the results have reasonably converged).

The concrete plates were modeled as a single first-order 8-node brick element (Element type 7) with linear material behavior. A Young's modulus of E=26 GPa and a Poisson ratio of ν=0.3 was considered. The elastomeric ball was modeled using second-order 10-node tetrahedral elements with a Herrmann variational principle for the displacement formulation (Element type 130). This type of element is preferred for elastomeric nearly-incompressible materials. Additional information about these elements (e.g., interpolation functions and integration points) can be found elsewhere [23]. The updated Lagrange formulation of the FE software was considered for the analyses.

A friction coefficient of μ=0.6 was considered for the interaction between the ball and concrete plates [24]; however, a parametric analysis showed that a larger coefficient of friction does not affect the results once the friction coefficient is large enough to restrain the ball from slipping with the surface.

The experimental tests were simulated by leaving the bottom plate fixed, increasing the vertical force in the top plate rampwise until it reached the target value, and then applying the horizontal displacement while restraining the motion in the undesired directions (e.g., rotations and out-of-plane translation).

3.3 Agreement between the tests and simulations

Figure 5 presents the deformed shape of the ball under the 12.5 kN of vertical force obtained in the finite element simulations and during the test. It is observed that the FE model could accurately represent the deformed shape of the ball, which could be mainly attributed to a good characterization of the equilibrium path of the material (nondissipative behavior). However, the energy dissipated during the rolling motion was not perfectly predicted.

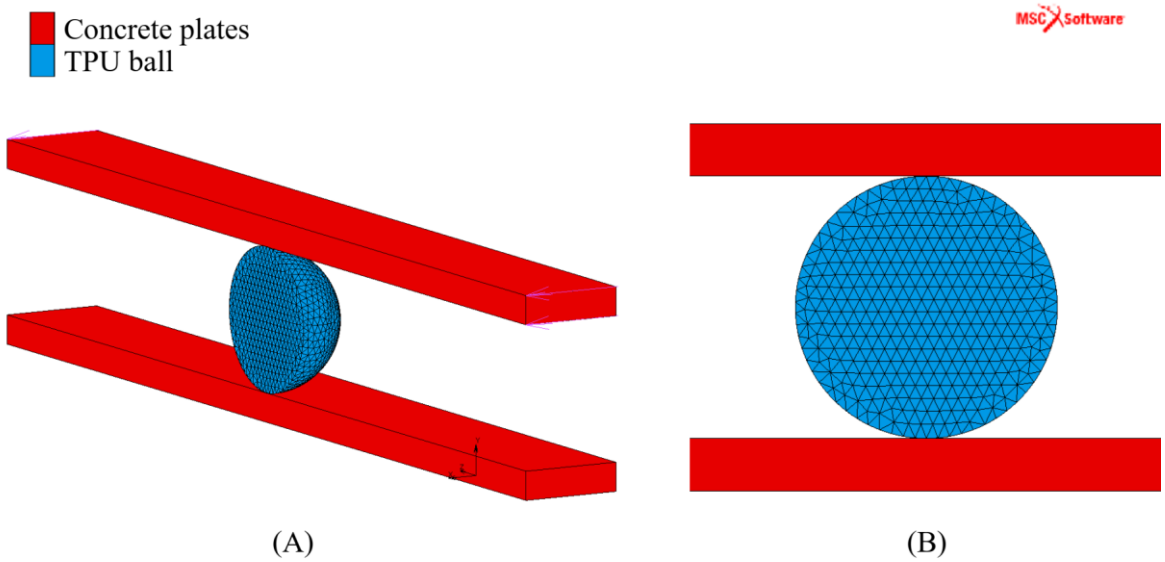

Figure 4: Finite element model: (A) Isometric view, and (B) frontal view.

Figure 6 shows the rolling resistance force and lateral displacement relationship obtained in the tests and the finite element simulation. It can be observed that although a similar amount of energy dissipated is observed in every cycle, the overall shape of the hysteretic loops is not the same. Two main differences can be highlighted for this level of deformations: i) The experimental test showed a small restoring force that is not observed in the finite element simulations, and ii) the unloading in the tests was less steep than in the numerical model.

These differences suggest that the considered material parameters are not optimal. The material parameters were obtained with testing protocols that represented the nonlinear behavior at a specific amplitude and rate of deformation [12]; however, this is not representative of the whole volume of the ball. Along the volume of the ball, some material points are deforming more than others, and also with different deformation rates. Therefore, a more detailed material characterization that considers different amplitudes and rates of deformations is required to obtain a reliable material parameter realization.

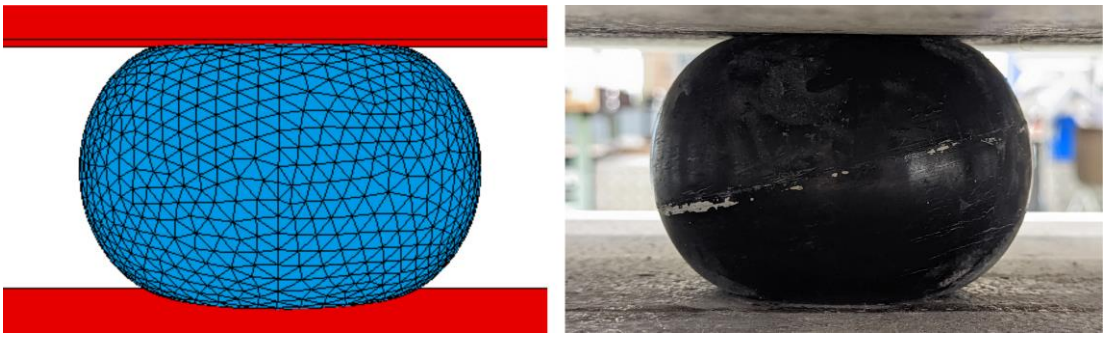

Figure 5: Deformed shape: Modeling vs. test.

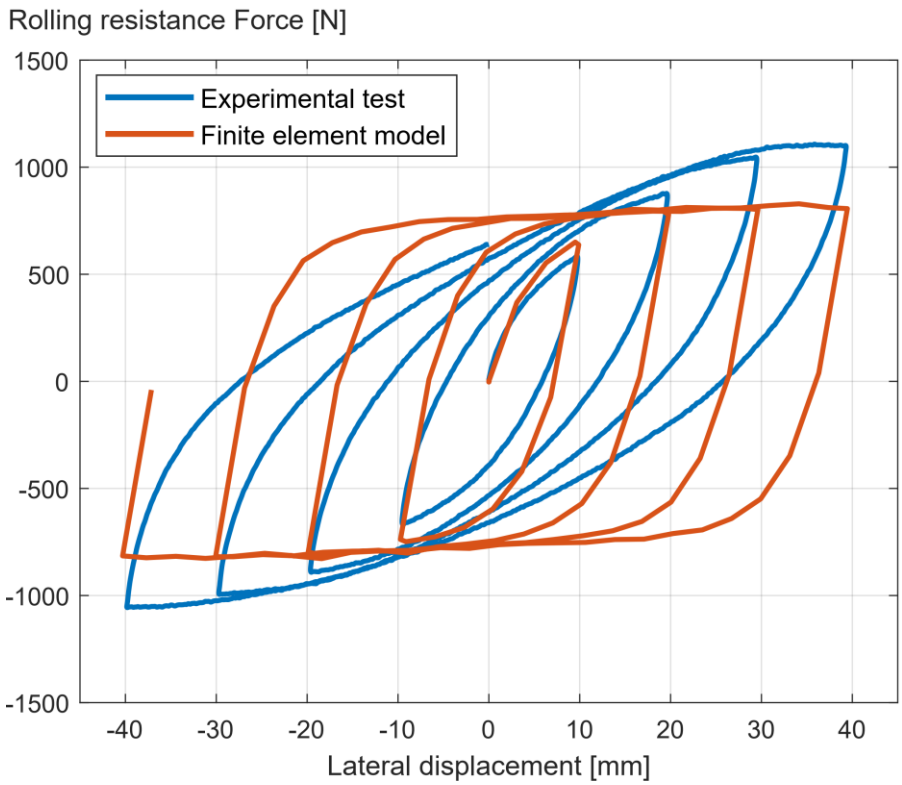

Figure 6: Rolling resistance force: Modeling vs. test.

4 CONCLUSIONS AND FINAL REMARKS

This paper presented the rolling behavior at small amplitudes of a TPU ball and its finite element simulation. The TPU ball was rolled between two concrete plates. A constant vertical force and a cyclic lateral displacement were applied to the top plate, simulating the induced displacement of the system caused by an earthquake motion. A parallel rheological framework with three mechanisms was considered to represent the constitutive material behavior of the ball using parameters based on a previous study. The obtained results allow drawing the following main conclusions:

- The finite element simulations could accurately represent the deformed shape of the ball under the vertical force. This may be associated with a good representation of the equilibrium path of the material.
- Despite having a good overall agreement, the model did not perfectly predict either the rolling resistance force or the energy dissipated. This suggests that the chosen parameter values did not allow the model to represent the mechanical deformations within the ball (in terms of amplitude and rate of deformation). This can be explained by the limited deformation protocols considered for obtaining the parameter values.
- Material model parameter values obtained with more suitable protocols (e.g., representing a broader range of deformations and rates) are required for better modeling performance.
- Further numerical analyses have to be performed at different loads and larger rolling deformations to understand the deformation mechanism to which the ball particles are subject.

ACKNOWLEDGMENTS

This research has been supported by the Sawiris Foundation for Social Development and ETH for Development. The authors are grateful for the support.

REFERENCES

1. Pinarbasi S, Mengi Y. Analysis of fiber-reinforced elastomeric isolators under pure "warping." *Structural Engineering and Mechanics* 2017; **61**(1): 31–47.
2. Kelly JM. Analysis of Fiber-Reinforced Elastomeric Isolators. *Journal of Seismology and Earthquake Engineering* 1999; **2**(1): 19–34.
3. Tsai HC, Kelly JM. Stiffness analysis of fiber-reinforced rectangular seismic isolators. *Journal of Engineering Mechanics* 2002; **128**(4): 462–470.
4. Osgooei PM, Tait MJ, Konstantinidis D. Seismic isolation of a shear wall structure using rectangular fiber-reinforced elastomeric isolators. *Journal of Structural Engineering (United States)* 2016; **142**(2).
5. Van Engelen NC, Konstantinidis D, Tait MJ. Structural and nonstructural performance of a seismically isolated building using stable unbonded fiber-reinforced elastomeric isolators. *Earthquake Engineering and Structural Dynamics* 2016; **45**(3): 421–439.
6. Tsai CS, Lin YC, Chen WS, Su HC. Tri-directional shaking table tests of vibration sensitive equipment with static dynamics interchangeable-ball pendulum system. *Earthquake Engineering and Engineering Vibration* 2010; **9**(1): 103–112.
7. Tsai CS, Lin YC, Chen WS, Tsou CP, Chen MJ. The material behavior and isolation

benefits of ball pendulum system. *American Society of Mechanical Engineers, Pressure Vessels and Piping Division (Publication) PVP*, vol. 2006, 2006.

8. Cilsalar H, Constantinou MC. Parametric study of seismic collapse performance of lightweight buildings with spherical deformable rolling isolation system. *Bulletin of Earthquake Engineering* 2020; **18**(4): 1475–1498.
9. Cilsalar H, Constantinou MC. Behavior of a spherical deformable rolling seismic isolator for lightweight residential construction. *Bulletin of Earthquake Engineering* 2019; **17**(7): 4321–4345.
10. Katsamakas AA, Belser G, Vassiliou MF, Blondet M. Experimental investigation of a spherical rubber isolator for use in low income countries. *Engineering Structures* 2022; **250**: 113522.
11. Katsamakas AA, Vassiliou MF. Experimental Parametric Study and Phenomenological Modeling of a Deformable Rolling Seismic Isolator. *Journal of Earthquake Engineering* 2023: 1–30.
12. Reyes S, Vassiliou M, Agathos K, Konstantinidis D. *Effects of two testing protocols on the material model parameter identification for rubber-like materials*. Romania: Editura Conspress; 2022.
13. Bergstrom JS. *Mechanics of solid polymers: theory and computational modeling*. 2015th ed. William Andrew, ElSevier; 2015.
14. Yeoh OH. Some forms of the strain energy function for rubber. *Rubber Chemistry and Technology* 1993; **66**(5): 754–771.
15. Arruda EM, Boyce MC. A three-dimensional constitutive model for the large stretch behavior of rubber elastic materials. *Journal of the Mechanics and Physics of Solids* 1993; **41**(2): 389–412.
16. Marc M. Volume A : Theory and User Information. *MSC Software Corporation, Palo Alto, USA* 2019: 867.
17. Bergström JS, Boyce MC. Mechanical behavior of particle filled elastomers. *Rubber Chemistry and Technology* 1999; **72**(4): 633–656.
18. Bergström J. Large strain time-dependent behavior of elastomeric materials. *PhD Thesis* 1999: 260.
19. Bergström JS, Boyce MC. Large strain time-dependent behavior of filled elastomers. *Mechanics of Materials* 2000; **32**(11): 627–644.
20. Bergström JS, Boyce MC. Constitutive modeling of the large strain time-dependent behavior of elastomers. *Journal of the Mechanics and Physics of Solids* 1998; **46**(5): 931–954.
21. Bergström JS, Boyce MC. Constitutive modeling of the time-dependent and cyclic loading of elastomers and application to soft biological tissues. *Mechanics of Materials* 2001; **33**(9): 523–530.
22. MSC Software Corporation. MSC Marc 2019.
23. Marc M. Volume B: Element Library. *MSC Software Corporation, Palo Alto, USA* 2019: 949.
24. Lorenz B, Persson BNJ, Dieluweit S, Tada T. Rubber friction: Comparison of theory with experiment. *European Physical Journal E* 2011; **34**(12): 111–129.